Spectroscopy of Ru(II) polypyridyl complexes used as intercalators in DNA: Towards a theoretical study of the light switch effect

ARTICLE *in* JOURNAL OF PHOTOCHEMISTRY AND PHOTOBIOLOGY A CHEMISTRY · AUGUST 2007

Impact Factor: 2.5 · DOI: 10.1016/j.jphotochem.2007.01.015

3 AUTHORS, INCLUDING:

Leticia González
University of Vienna
210 PUBLICATIONS **3,380** CITATIONS
SEE PROFILE

Chantal Daniel
University of Strasbourg
124 PUBLICATIONS **2,244** CITATIONS
SEE PROFILE

Available online at www.sciencedirect.com
ScienceDirect
Journal of Photochemistry and Photobiology A: Chemistry 190 (2007) 310–320
Journal of Photochemistry and Photobiology A:Chemistry
www.elsevier.com/locate/jphotochem

Spectroscopy of Ru(II) polypyridyl complexes used as intercalators in DNA: Towards a theoretical study of the light switch effect

Michiko Atsumi [a,c], Leticia González [b], Chantal Daniel [c,*]

[a] *Graduate School of Humanities and Sciences, Ochanomizu University, 2-1-1 Otsuka, Bunkyo-ku, Tokyo 112-8610, Japan*
[b] *Institut für Chemie und Biochemie, Freie Universität Berlin, Takustr. 3, 14195, Germany*
[c] *Laboratoire de Chimie Quantique, Institut de Chimie UMR 7177 CNRS/Université Louis Pasteur 4 Rue Blaise Pascal, 67000 Strasbourg, France*

Received 10 October 2006; received in revised form 14 December 2006; accepted 16 January 2007
Available online 21 January 2007

Abstract

The absorption spectroscopy of $[Ru(phen)_2dppz]^{2+}$ and $[Ru(tap)_2dppz]^{2+}$ (phen = 1,10-phenanthroline, tap = 1,4,5,8-tetraazaphenanthrene; dppz = dipyridophenazine) complexes used as molecular light switches by intercalation in DNA has been analysed by means of Time-Dependent Density Functional Theory (TD-DFT). The electronic ground state structures have been optimized at the DFT (B3LYP) level of theory. The absorption spectra are characterized by a high density of excited states between 500 nm and 250 nm. The absorption spectroscopy of $[Ru (phen)_2dppz]^{2+}$ in vacuum is characterized by metal-to-ligand-charge-transfer (MLCT) transitions corresponding to charge transfer from Ru(II) either to the phen ligands or to the dppz ligand with a strong MLCT ($d_{Ru} \rightarrow \pi^*_{dppz}$) absorption at 411 nm. In contrast, the main feature of the lowest part of the vacuum theoretical spectrum of $[Ru(tap)_2dppz]^{2+}$ between 522 nm and 400 nm is the presence of various excited states such as MLCT ($d_{Ru} \rightarrow \pi^*_{TAP}$), ligand-to-ligand-charge-transfer LLCT ($\pi_{dppz} \rightarrow \pi^*_{TAP}$) or intra-ligand IL ($\pi_{dppz} \rightarrow \pi^*_{dppz}$) states. When taking into account solvent corrections within the polarizable continuum model (PCM) approach (H_2O, CH_3CN) the absorption spectrum of $[Ru(tap)_2dppz]^{2+}$ is dominated by a strong absorption at 388 nm (CH_3CN) or 390 nm (H_2O) assigned to a ^{1}IL ($\pi_{dppz} \rightarrow \pi^*_{dppz}$) corresponding to a charge transfer from the outside end of the dppz ligand to the site of coordination to Ru(II). These differences in the absorption spectra of the two Ru(II) complexes have dramatic effects on the mechanism of deactivation of these molecules after irradiation at about 400 nm. In particular, the electronic deficiency at the outside end of the dppz ligand created by absorption to the ^{1}IL state will favour electron transfer from the guanine to the Ru(II) complex when it is intercalated in DNA.

Keywords: Spectroscopy; Ruthenium polypyridyl; Photophysics; Theoretical chemistry; DNA intercalators

1. Introduction

Increasing attention has been devoted to the design of new transition metal complexes as potential probes for nucleic acids since the discovery in 1990 of $[Ru(bpy)_2(dppz)]^{2+}$ highly sensitive luminescent reporter of double-helical DNA [1]. The investigation of photophysical, electrochemical and structural properties of novel Ru(II) complexes in the presence and absence of DNA has pointed to their potential as "molecular light switches" [2,3]. It has been found that the photoluminescence quantum yields of these complexes are extremely sensitive to the environment [1–3]. In particular, when DNA is added to an aqueous solution of the complexes the yield of emission increases dramatically. It was proposed that few triplets metal-to-ligand-charge-transfer (MLCT) $d_{Ru} \rightarrow \pi^*_{dppz}$ excited states give rise to the DNA light switch effect in these systems [4–6]. Moreover, the luminescent parameters are remarkably sensitive to the DNA structure and binding modes at intercalation [1–3]. The chemical properties of these coordinatively saturated molecules which are water soluble and inert to substitution make them excellent compounds as diagnostic and therapeutic agents [2]. These molecules have also been exploited in the study of electron transfer between the base pairs of DNA. As illustrated by a recent review article on ruthenium polypyridyl chemistry [7] this area of research has opened the route to a wide range of applications in various fields. Experiments reported on $[Ru(tap)_2dppz]^{2+}$ and $[Ru(phen)_2dppz]^{2+}$ have shown that these Ru(II) complexes strongly bind to dou-

* Corresponding author. Tel.: +33 3 90 24 13 14; fax: +33 3 90 24 15 89.
E-mail address: daniel@quantix.u-strasbg.fr (C. Daniel).

1010-6030/$ – see front matter © 2007 Elsevier B.V. All rights reserved.
doi:10.1016/j.jphotochem.2007.01.015

ble helical DNA being very efficient "molecular light switches" [4,8–14]. Linear dichroism spectroscopy [8–10], steady-state as well as time-resolved absorption/emission spectroscopy and laser flash photolysis experiments [4,11,12] have investigated the properties of $[Ru(tap)_2L]^{2+}$ (L = bpy, phen, tap, dppz) and of $[Ru(phen)_2dppz]^{2+}$ in DNA, in different solvents (H_2O, CH_3CN, H_2O/CH_3CN mixture) and in various double-stranded synthetic polynucleotides, such as $[poly(dA\text{-}dT)]_2$ and $[poly(dG\text{-}dC)]_2$. The first example of *reversible* DNA light switch has been recently accomplished for $[Ru(byp)_2(tpphz)]^{2+}$ (tpphz = tetrapyrido phenazine) [15]. The experimental spectrum of $[Ru(phen)_2dppz]^{2+}$ is characterized by an absorption in the visible region assigned to a metal-to-ligand-charge-transfer MLCT transition (λ_{max} = 440 nm) and to an intraligand IL transition localized on the dppz chromophore (λ_{max} = 372 nm; ε = 21 800 M^{-1} cm^{-1}) [13]. The emission yield is undetectable in water, but moderate in acetonitrile and increases when the complex is intercalated to DNA or bound to polynucleotides [4,11,12]. The efficient quenching of luminescence in water has been proposed to be due to fast hydrogen bonding of solvent to the phenazine aza nitrogens of the dppz anion radical (formed in the MLCT states) [16–18]. Methyl substitution effects on the radiative and solvent quenching rate constants on $[Ru(phen)_2dppz]^{2+}$ have been investigated by Olofsson et al. [19]. When the distant benzene ring of the dppz ligand is substituted by methyl groups a dramatic increased luminescence lifetimes and quantum yield in polyol solvents is observed. A similar effect, but less dramatic is observed when the substituted complexes are intercalated in DNA. The substitution has no effect on the position and intensity of the MLCT band at 440 nm, but the perturbation of the dppz chromophore is significant in the IL band [19]. Pure enantiomers Δ and Λ of $[Ru(phen)_2dppz]^{2+}$ have been synthesized and it has been shown that the Δ enantiomer is primarily responsible for the luminescence enhancement upon DNA binding reported for the racemate [14]. Interestingly, a recent study has shown that the luminescence of both the Δ and Λ forms of the $[Ru(phen)_2dppz]^{2+}$ is enhanced not only upon intercalation with DNA but also when the metal complexes bind to single stranded oligonucleotides [20].

The behaviour of the tap substituted complexes is characterized by the presence of excited states able to oxidise guanine.

$$[Ru(tap)_2(L)]^{2+*} + G \rightarrow [Ru(tap)_2(L)]^{+} + G^{\bullet +} \quad (1)$$

This photo-induced electron transfer is a key step in the enhancement of strand breaks and in adducts formation such as nucleobase and mononucleotide derivatives [11]. UV/vis transient experiments on $[Ru(tap)_2dppz]^{2+}$ in aqueous buffer or intercalated in polynucleotides [12] point to the presence of a shoulder between 400 nm and 500 nm and a strong absorption at 278 nm. The strong IL band observed in $[Ru(phen)_2dppz]^{2+}$ and in the free dppz ligand between 350–400 nm is not visible in $[Ru(tap)_2dppz]^{2+}$. In the presence of $[poly(dG\text{-}dC]_2$ the luminescence of $[Ru(tap)_2dppz]^{2+}$ is quenched and $[Ru(tap)_2dppz]^{+}$ is formed within 480 ± 40 ps, through electron transfer from the guanine to the excited state, as evidenced by means of a 400 fs pulse of 400 nm light by Kelly et al. [12].

Most of the theoretical studies performed until now have focus either on the structural or binding aspects [21] or on the nature and position of the low-lying triplet excited states in order to interpret the emission spectroscopy [22–25]. Structural and binding modes have been studied by means of force field approaches showing a classical intercalation for $[Ru(phen)_2dppz)]^{2+}$ [21]. The spectroscopic calculations reported on $[Ru(phen)_2dppz]^{2+}$ were based essentially on semi-empirical methods [22,23] and TD-DFT [24,25] studies. It has been shown that the low-lying MLCT states delocalized over the three ligands in the free complex slightly red-shifted and relocalize on the different ligands (phen or dppz) upon binding to DNA [22]. Recent DFT/TD-DFT analysis have assigned the experimental band characterized at 440 nm to a superposition of two distinct MLCT features, which arise from two groups of transitions, one at ≈450 nm and another at ≈415 nm, which correspond to $d_{Ru} \rightarrow \pi^*_{dppz}$ and $d_{Ru} \rightarrow \pi^*_{phen}$, respectively. The band at ≈372 nm has been assigned to have a dominant MLCT character partially mixed with dppz IL [24]. INDO/SCI calculations completed by TD-DFT on a series of polyazaaromatic Ru(II) complexes have shown that molecules containing π-extended ligands, such as dppz, are characterized by luminescence lifetimes largely dependent on temperature in aprotic solvents. This behaviour has been associated to the presence of low-lying triplet IL states centred mainly on the π-extended ligand [23]. Finally, TD-DFT calculations of the low-lying triplet excited states of $[Ru(bpy)_2dppz]^{2+}$ without and with solvent effects point to the presence of low-lying ^{3}MLCT ($d_{Ru} \rightarrow \pi^*_{bpy}$) states in gas phase which are delocalized within the dppz ligand when solvent correction is included [25]. This effect has been attributed to a change in dipole moment of the molecule. The lowest triplet state has been assigned to a ^{3}IL ($\pi_{dppz} \rightarrow \pi^*_{dppz}$).

The aim of the present study is to analyze and rationalise the absorption/emission spectroscopy in $[Ru(phen)_2dppz)]^{2+}$ and $[Ru(tap)_2dppz]^{2+}$ which are used as DNA intercalators in luminescence experiments. Our objective is to propose a qualitative mechanism able to explain the occurrence of competing processes under visible irradiation, namely luminescence versus electron transfer. For this purpose we performed a detailed investigation of the early stage photophysics (within ∼10 ps) of these two molecules. This is a preliminary step towards the fundamental understanding of the light switch effect in this class of molecules.

2. Computational details

The geometrical structures of $[Ru(L)_2(L')]^{2+}$ complexes (L = L′ = tap; L = phen, L′ = dppz; L = tap, L′ = dppz) were optimized in vacuum for the closed shell electronic ground state at the DFT (B3LYP) [26] level within C_1 symmetry. The following basis sets and pseudopotentials describing the core electrons of the metal centre were used: (i) a full double-ξ D95 basis set (9s, 5p) contracted to [4s,2p] for C and N atoms and (4s) contracted to [2s] for H atoms [27] combined to LanL2DZ effective core potentials and associated valence basis sets for the Ru atom [28] (denoted as BSI); (ii) a polarized split valence 6-31G* basis set

(10s, 4p, 1d) contracted to [3s, 2p, 1d] for C and N atoms and (4s) contracted to [2s] for H atoms [29] with Wood–Boring quasi relativistic MWB pseudopotentials and associated valence basis sets (8s, 7p, 6d) contracted to [6s, 5p, 3d] for the Ru atom [30] (denoted as BSII); (iii) a full double-ξ D95 basis set (9s, 5p) contracted to [4s, 2p] for C and N atoms and (4s) contracted to [2s] for H atoms [27] combined with Wood-Boring quasi relativistic MWB pseudopotentials and associated valence basis sets (8s, 7p, 6d) contracted to [6s, 5p, 3d] for the Ru atom [30] (denoted as BSIII). The second set (BSII) has been used for further structural studies as well as for the excited states calculations of $[Ru(tap)_2dppz]^{2+}$ and $[Ru(phen)_2dppz]^{2+}$.

The theoretical electronic absorption spectra have been obtained by means of Time Dependent DFT method (TD-DFT) [31] applied to the optimized geometrical structures of the electronic ground state for both complexes. The geometries of the triplet electronic excited states have not been optimized since we focus here on electronic absorption spectroscopy and photophysical processes occurring in a short time-scale (less than 10 ps) where nuclear relaxation effects can be neglected. The choice of the method is governed by the size of the molecules and our wish to investigate environment effects in future work. Whereas DFT (B3LYP) is the method of choice for structures determination of large transition metal complexes in their electronic ground states [32], the failure of TD-DFT for long-range CT excited states is well established and has been discussed in a number of recent articles [33–37]. According to our experience in large transition metal complexes MLCT states are well described [38–41]. The TD-DFT spectra of $[Re(CO)_3(2,2'\text{-bipyridine})(t\text{-4-styrylpyridine})]^+$ [38], $[Ru(E)(E')(CO)_2(iPr\text{-DAB})]$ (E = E′ = $SnPh_3$ or Cl; E′ = CH_3; iPr-DAB = *N*,*N*′-di-isopropyl-1,4-diaza-1,3-butadiene) [39], $[Ru(X)(Me)(CO)_2(\alpha\text{-diimine})]$ (X = Cl, I; α-diimine = Me-DAB; iPr-DAB; DAB = 1,4-diaza-1,3-butadiene) [40,41] and of the series $[Ru(phen)_2(bpy)]^{2+}$, $[Ru(phen)_2(dmbp)]^{2+}$, $[Ru(tpy)(phen)(CH_3CN)]^{2+}$, and $[Ru(tpy)(dmp)(CH_3CN)]^{2+}$ [42] have been validated by comparison with the experimental spectra [38,39,42] and in some cases with accurate CASSCF/CASPT2 calculations [38–41]. The effect of increasing Hartree–Fock exchange in the functional on calculated transition energies has been investigated in detail for $[Ru(X)(Me)(CO)_2(\alpha\text{-diimine})]$ [41]. In the case of $[Re(CO)_3(2,2'\text{-bipyridine})(t\text{-4-styrylpyridine})]^+$ [38], even if the presence of low-lying long range ligand-to-ligand-charge-transfer (LLCT) states, not observed in the experimental spectrum, has been attributed to an artefact of the TD-DFT method, the description of the MLCT and intra-ligand (IL) states is generally correct. Nevertheless, it has been shown that the failure of the Kohn–Sham theory at describing transition metal–halide bonding in $[Ru(Cl)(Me)(CO)_2(\alpha\text{-diimine})]$ leads to a wrong TD-DFT assignment of the lowest excited states, which overestimates the halide (X = Cl) to ligand charge transfer (XLCT) character in detriment to the MLCT character [40,41]. The electronic spectra of the complexes under investigation in the present work are essentially characterized by MLCT and IL excited states, while the LLCT states play a minor role in the electronic absorption spectroscopy and in the photophysics.

In our calculations, 75 excited states have been obtained but only the states with significant oscillator strengths (>0.01) will be reported. An investigation of the solvent effects on the optimized structures and on the absorption spectroscopy has been performed with the crude polarizable continuum model (PCM) within the Integral-Equation-Formalism (IEFPCM) [43–45] for CH_3CN ($\varepsilon = 36.64$) and H_2O ($\varepsilon = 78.39$) with BSII.

All the calculations are performed with Gaussian 03 quantum chemistry software [46].

3. Results and discussion

3.1. Structure of $[Ru(tap)_3]^{2+}$, $[Ru(tap)_2dppz]^{2+}$ and $[Ru(phen)_2dppz]^{2+}$

The DFT(B3LYP) optimized geometries of the $[Ru(tap)_3]^{2+}$, $[Ru(tap)_2dppz]^{2+}$and $[Ru(phen)_2dppz]^{2+}$ complexes in vacuum are reported in Table 1 and depicted in Fig. 1a–c, respectively. The optimized geometry of $[Ru(tap)_3]^{2+}$ is compared to the experimental X-ray structure [47] and the optimized geometry of $[Ru(phen)_2dppz]^{2+}$ is compared to the X-ray structure of

Table 1
DFT (B3LYP) optimized bond lengths (in Å) and bond angles (in °) of $[Ru(tap)_3]^{2+}$, $[Ru(tap)_2dppz]^{2+}$ and $[Ru(phen)_2dppz]^{2+}$ complexes and X-ray data for $[Ru(tap)_3]^{2+}$ [47] and $[Ru(dmp)_2dppz]^{2+}$[Ref [48]]

	X-ray	$[Ru(tap)_3]^{2+}$			$[Ru(tap)_2dppz]^{2+}$			$[Ru(phen)_2dppz]^{2+}$			Ref. [25]
		BSI	BSII	BSIII	BSI	BSII	BSIII	BSI	BSII	BSIII	X-ray
$Ru-N_1$	2.06	2.01	2.11	2.10	2.04	2.11	2.10	2.02	2.11	2.10	2.094
$Ru-N_2$	2.08	2.01	2.11	2.10	2.04	2.11	2.10	2.02	2.11	2.10	2.098
$Ru-N_3$	2.06	2.01	2.11	2.10	2.00	2.11	2.09	2.01	2.11	2.10	2.096
$Ru-N_4$	2.05	2.01	2.12	2.10	2.00	2.12	2.10	2.01	2.11	2.10	2.109
$Ru-N_5$	2.06	2.01	2.11	2.10	2.00	2.12	2.10	2.01	2.11	2.10	2.102
$Ru-N_6$	2.08	2.01	2.11	2.10	2.00	2.11	2.09	2.01	2.11	2.10	2.125
N_1RuN_2	79.4	81.1	79.3	80.1	80.2	78.7	79.4	80.5	78.6	78.9	78.86
N_1RuN_4	175.1	170.4	173.0	173.2	169.4	172.9	173.0	170.4	173.2	173.2	–
N_2RuN_5	169.8	170.4	173.0	173.4	169.4	172.9	173.0	170.4	173.2	173.2	–
N_3RuN_4	80.4	81.1	79.3	80.1	81.3	79.4	80.2	80.8	78.8	79.2	78.85
N_3RuN_6	172.3	170.4	173.0	173.4	172.6	173.8	174.1	171.1	173.2	173.2	–
N_5RuN_6	80.6	81.1	79.4	80.1	81.3	79.4	80.2	80.8	78.8	79.2	79.41

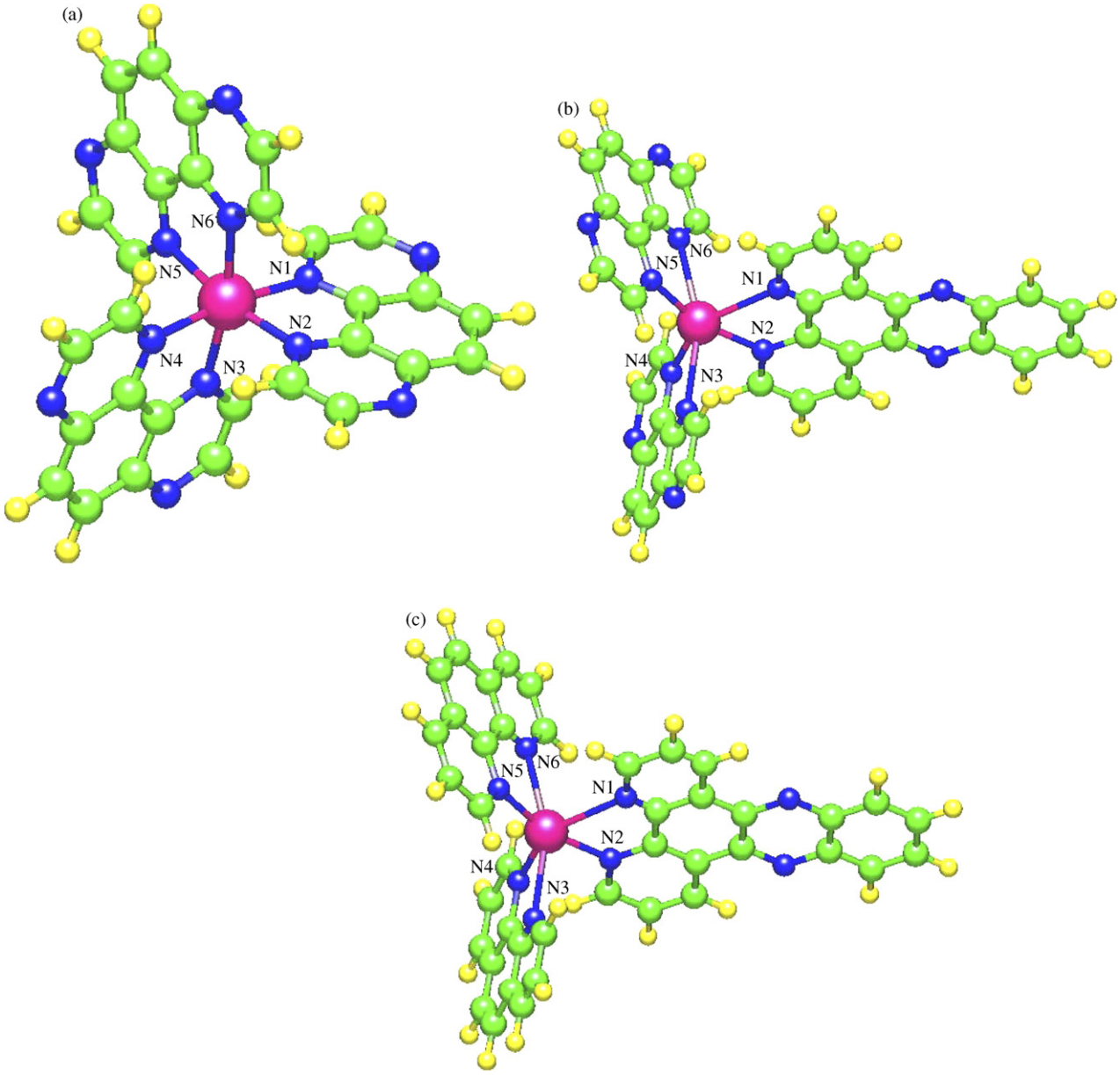

Fig. 1. Optimized structures of $[Ru(tap)_3]^{2+}$ (a), $[Ru(tap)_2dppz]^{2+}$ (b) and $[Ru(phen)_2dppz]^{2+}$ (c).

$[Ru(dmp)_2dppz]^{2+}$ (dmp = 2,9-dimethyl 1,10-phenanthroline), which is the closest experimentally characterized complex [48].

The geometries of the three complexes do not differ drastically. The Ru–N bond lengths are slightly overestimated (∼0.05 Å) by the DFT optimization, regardless of BSII or BSIII; this is illustrated in the theoretical bond lengths of $[Ru(tap)_3]^{2+}$ and $[Ru(phen)_2dppz]^{2+}$ as compared to the X-ray data. The calculations performed with BSI using LanL2DZ effective core potentials on the Ru atom underestimate dramatically the Ru–N bonds distances. Otherwise the bond angles are not really affected by the choice of the basis sets and associated effective core potentials.

The opening of the N_1–Ru–N_4 angle correlated to the closing of the N_2–Ru–N_5 angle in $[Ru(tap)_3]^{2+}$ is not reproduced by the calculations. The optimization converges to pseudo-octahedral symmetry with N–Ru–N angles close to 80°. The N_1–Ru–N_4 and N_2–Ru–N_5 angles which connect the dppz ligand to the external ligands (tap or phen) are nearly identical and do not differ from the tap to the phen complexes with values close to 173° corresponding to an opening of the structure as compared to the one of $[Ru(tap)_3]^{2+}$ which does not possess an extended ligand. The N_3–Ru–N_6 angle connecting the two external ligands amounts to values close to 173° slightly overestimated with respect to the experimental value of 172.3° in $[Ru(tap)_3]^{2+}$. While experimental structures are characterized by different Ru–N(phen) or Ru–N(tap) bond lengths all the Ru–N optimized distances show similar values in the range 2.10–2.11 Å comparable to the average experimental Ru–N bond lengths, namely 2.065 Å for $[Ru(tap)_3]^{2+}$ and 2.104 Å for $[Ru(dmp)_2dppz]^{2+}$.

Table 2
DFT (B3LYP) optimized bond lengths (in Å) and bond angles (in °) of $[Ru(tap)_2dppz]^{2+}$ and $[Ru(phen)_2dppz]^{2+}$ complexes without and with PCM solvent correction with BSII (CH_3CN; $\varepsilon = 36.64$, H_2O; $\varepsilon = 78.39$)

	$[Ru(tap)_2dppz]^{2+}$			$[Ru(phen)_2dppz]^{2+}$		
	Vacuum	CH_3CN	H_2O	Vacuum	CH_3CN	H_2O
$Ru—N_1$	2.113	2.106	2.110	2.11	2.107	2.105
$Ru—N_2$	2.113	2.105	2.110	2.11	2.105	2.104
$Ru—N_3$	2.106	2.098	2.099	2.11	2.108	2.106
$Ru—N_4$	2.115	2.107	2.108	2.11	2.108	2.105
$Ru—N_5$	2.115	2.108	2.109	2.11	2.106	2.105
$Ru—N_6$	2.106	2.098	2.101	2.11	2.107	2.105
N_1RuN_2	78.7	78.8	78.6	78.6	78.6	78.7
N_1RuN_4	172.9	172.97	173.3	173.2	173.8	173.8
N_2RuN_5	172.9	173.2	173.3	173.2	173.7	173.7
N_3RuN_4	79.4	79.59	79.5	78.8	79.02	79.1
N_3RuN_6	173.8	174.12	174.1	173.2	173.0	172.8
N_5RuN_6	79.4	79.6	79.5	78.8	79.12	79.2

When solvent correction is added (H_2O, CH_3CN) the bond lengths are slightly contracted but the overall theoretical structure is not drastically affected, as illustrated by the results reported in Table 2.

3.2. Electronic structure of $[Ru(tap)_2dppz]^{2+}$ and $[Ru(phen)_2dppz]^{2+}$

The electronic structure of the ground states of $[Ru(tap)_2dppz]^{2+}$ (374 electrons) and $[Ru(phen)_2dppz]^{2+}$ (378 electrons) complexes is ^1A (d^6 on Ru(II)) with the Kohn–Sham (KS) orbitals depicted in Fig. 2a and b, respectively. In both complexes, the Kohn–Sham orbitals are well localized either on the external ligands, or on the dppz ligand. The seven low-lying π* orbitals localized either on the tap, the phen or the dppz ligands are nearly pure. The π system (π_{dppz}, π_{tap}, π^*_{dppz}, π^*_{tap}) is stabilized by the presence of two extra nitrogen atoms at the positions 5 and 8 of the phen ligand (tap complex). The three low-lying $4d_{Ru}$ occupied orbitals are stabilized when going from the phen to the tap complex by a more favourable interaction with the dppz ligand. In the case of the tap substituted molecule the HOMO, HOMO-1 and HOMO-3 correspond to π_{dppz} orbitals and the HOMO-2 corresponds to $4d_{Ru}$ orbitals. The π_{tap} occupied orbitals are lowest in energy. The lowest vacant orbitals, until LUMO +3 correspond to π* orbitals localized on the tap ligand, whereas the upper vacant orbitals correspond to π^*_{dppz} orbitals. The HOMO–LUMO energy gap is 0.10 a.u.

The HOMO–LUMO energy gap amounts at 0.13 a.u. in $[Ru(phen)_2dppz]^{2+}$ where the $4d_{Ru}$ are significantly destabilized with respect to those of the tap complex due to a less favourable interaction with the dppz ligand. The HOMO is also a π_{dppz} orbital but the HOMO-1, HOMO−2 and HOMO-3 correspond to $4d_{Ru}$ orbitals. In contrast to $[Ru(tap)_2dppz]^{2+}$, the HOMO and HOMO−1 are nearly degenerate. The LUMO and LUMO+1 correspond to π* orbitals localized on the external phen ligands. According to the scheme of KS orbitals depicted in Fig. 2, the lowest metal to ligand charge transfer states should correspond to excitations to the external ligands, either tap or phen, depending on the complex. Moreover, a stabilization of the MLCT ($4d_{Ru} \rightarrow \pi^*_{dppz}$) states should be observed in $[Ru(phen)_2dppz]^{2+}$. The three $4d_{Ru}$ orbitals are nearly degenerate in the phen complex whereas this degeneracy is partially lifted in the tap complex by interaction with the dppz ligand. Considering only the set of 14 orbitals depicted in Fig. 2, a large number of electronic excited states can be generated by single excitation leading to a high density of states in the visible/UV domain of energy.

The KS orbitals of $[Ru(tap)_2dppz]^{2+}$ and $[Ru(phen)_2dppz]^{2+}$ complexes including the simple PCM solvent correction (for water and acetonitrile) are depicted in Fig. 3a and b, respectively. The qualitative character of the KS orbitals is not affected by the solvent correction and in both complexes we observe an overall destabilization of the orbitals. The $4d_{Ru}$ orbitals are destabilized whereas the π_{dppz} are stabilized with respect to each other. With solvent corrections the HOMO, corresponding to a π_{dppz} in vacuum, becomes metal localized in $[Ru(tap)_2dppz]^{2+}$ as well as in $[Ru(phen)_2dppz]^{2+}$.

3.3. Electronic absorption spectroscopy

The broad experimental absorption data in H_2O and CH_3CN [12,13] of the two Ru(II) complexes under investigation are reported in Table 3. The absorption spectrum of $[Ru(tap)_2dppz]^{2+}$ in H_2O is characterized by a shoulder with maxima at 412 nm and 458 nm and a stronger absorption starting at 366 nm, followed by a first intense band at 278 nm and a second one starting at 230 nm [12]. In acetonitrile only the

Table 3
Experimental absorption data (λ_{max} in nm) for $[Ru(tap)_2dppz]^{2+}$ and $[Ru(phen)_2dppz]^{2+}$ [13]

	H_2O	CH_3CN
$[Ru(tap)_2dppz]^{2+}$	230, 278, 366, 412, 458	278, 362, 412, 452
$[Ru(phen)_2dppz]^{2+}$	264, 278, 318, 358, 372, 440	264, 276, 316, 352,360, 368, 440

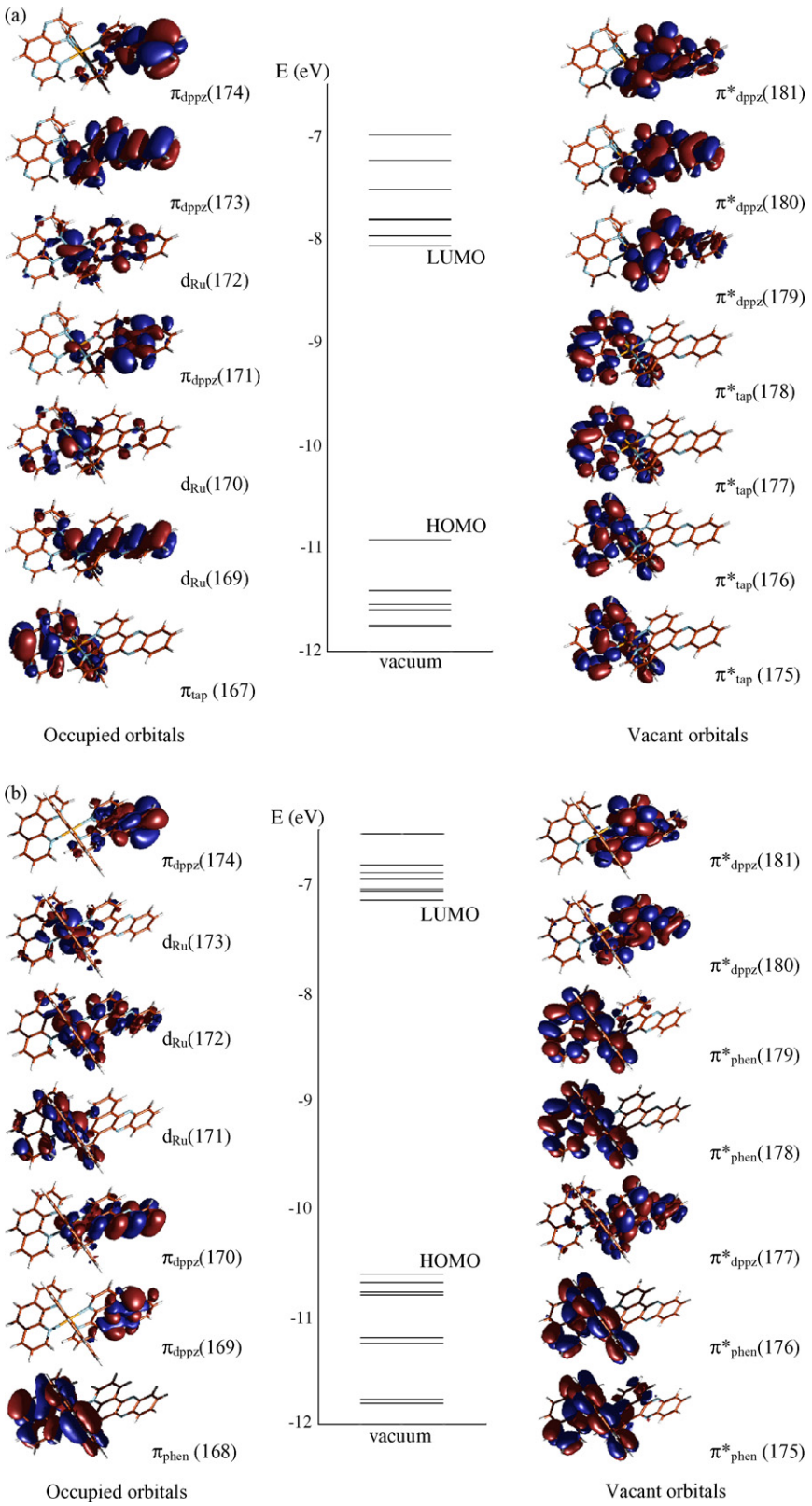

Fig. 2. Kohn–Sham electronic ground state orbitals of $[Ru(tap)_2dppz]^{2+}$ (a) and $[Ru(phen)_2dppz]^{2+}$ (b) in vacuum.

shoulder and the strong absorption starting at 362 nm with the intense band at 278 nm subsist. The upper band is not observed, for it is probably shifted to the blue. The absorption spectrum of $[Ru(phen)_2dppz]^{2+}$ is more crowded than the one of the tap complex and is not very sensitive to the solvent. Its main features are a band centred at 440 nm followed by two strong absorptions centred at 372 nm and 264 nm (in H_2O) and at 368 nm and 264 nm (in CH_3CN). A sequence of shoulders is

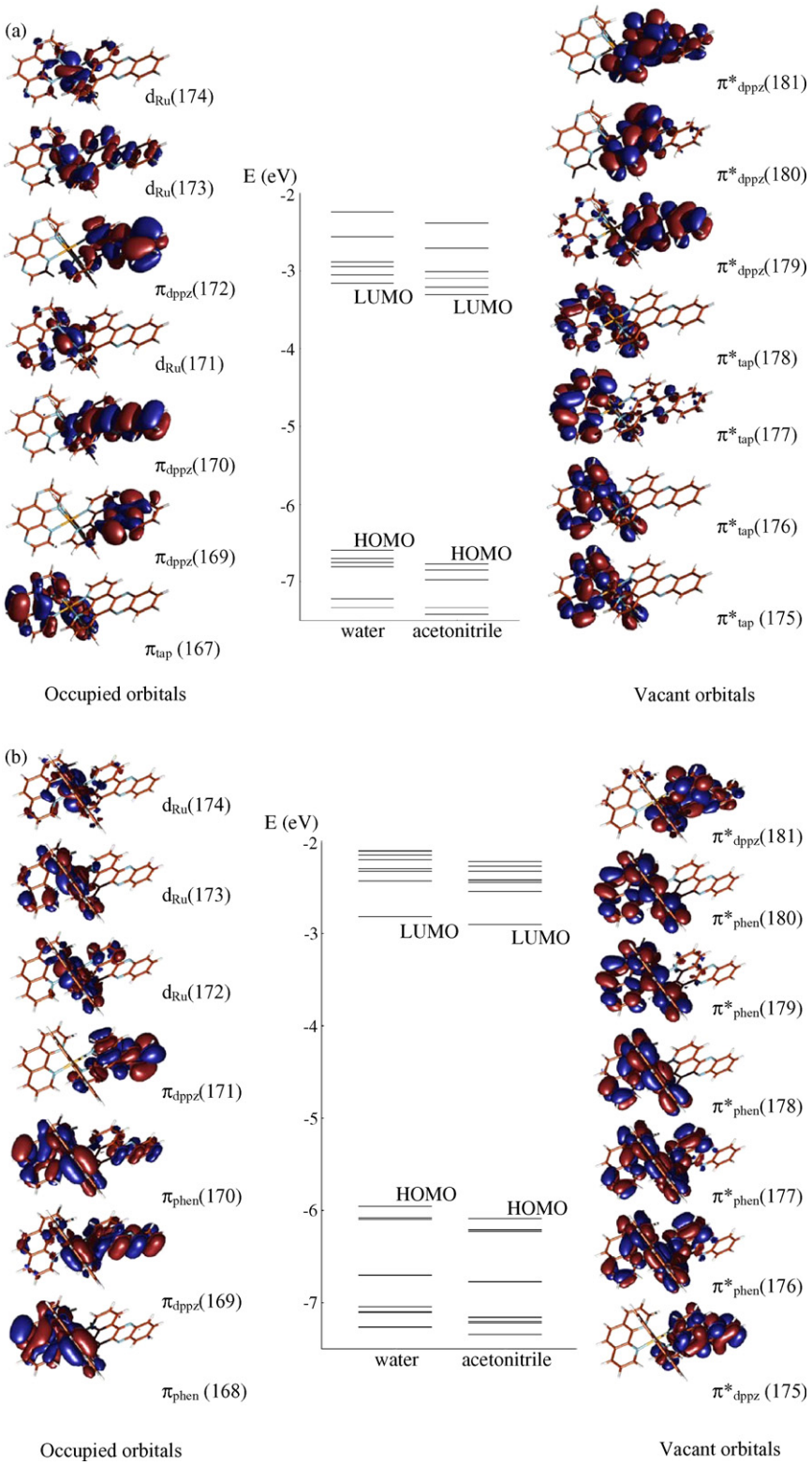

Fig. 3. Kohn–Sham electronic ground state orbitals of $[Ru(tap)_2dppz]^{2+}$ (a) and $[Ru(phen)_2dppz]^{2+}$ (b) solvent corrected for water and acetonitrile.

observed between 278–358 nm in H_2O and 276–360 in CH_3CN [13].

The theoretical absorption spectra of $[Ru(tap)_2dppz]^{2+}$ and $[Ru(phen)_2dppz]^{2+}$ in vacuum are reported in Tables 4 and 5, respectively. The theoretical absorption spectra of both complexes are characterized by a high density of states between 500 nm and 250 nm. Most of the charge transfer states are associated to very low oscillator strengths. Only the low-lying absorbing states with significant oscillator strengths ($\geq$0.01) are reported in Tables 4 and 5, which lie between 430 nm

Table 4
TD-DFT transition energies (in nm and eV) of the low-lying absorbing states ($f > 0.01$) of $[Ru(tap)_2dppz]^{2+}$ and associated oscillator strengths f (in vacuum)

nm	Transition	One-electron excitation[a]		f	eV
429	^{1}IL	$\pi_{dppz} \rightarrow \pi^*_{dppz}$	(174 → 179)	0.012	2.89
427	^{1}MLCT	$4d_{Ru} \rightarrow \pi^*_{tap}$	(170 → 175)	0.04	2.90
411	^{1}MLCT/^{1}LLCT	$4d_{Ru} \rightarrow \pi^*_{tap}/\pi_{dppz} \rightarrow \pi^*_{tap}$	(172 → 178)/(173 → 177)	0.015	3.01
406	^{1}LLCT	$\pi_{dppz} \rightarrow \pi^*_{tap}$	(173 → 178)	0.02	3.06
401	**^{1}LLCT**	$\mathbf{\pi_{dppz} \rightarrow \pi^*_{tap}}$	(173 → 177)	**0.1**	**3.09**
386	^{1}MLCT/^{1}LLCT	$4d_{Ru} \rightarrow \pi^*_{tap}/\pi_{dppz} \rightarrow \pi^*_{tap}$	(169 → 176)/(173 → 176)	0.03	3.21
383	^{1}MLCT	$4d_{Ru} \rightarrow \pi^*_{tap}$	(170 → 178)	0.02	3.24
382	**^{1}IL**	$\pi_{dppz} \rightarrow \pi^*_{dppz}$	(173 → 179)	**0.18**	**3.24**
372	^{1}IL	$\pi_{dppz} \rightarrow \pi^*_{dppz}$	(174 → 181)	0.06	3.33
364	^{1}MLCT	$4d_{Ru} \rightarrow \pi^*_{tap}$	(169 → 177)	0.01	3.41
362	^{1}MLCT	$4d_{Ru} \rightarrow \pi^*_{tap}$	(169 → 178)	0.05	3.43
324	**^{1}MLCT/^{1}IL**	$4d_{Ru} \rightarrow \pi^*_{dppz}/\pi_{dppz} \rightarrow \pi^*_{dppz}$	(172 → 181)/(173 → 180)	**0.19**	**3.83**
318	^{1}IL	$\pi_{dppz} \rightarrow \pi^*_{dppz}$	(173 → 181)	0.02	3.90
316	^{1}LLCT	$\pi_{dppz} \rightarrow \pi^*_{tap}$	(168 → 176)	0.01	3.92
311	^{1}IL	$\pi_{tap} \rightarrow \pi^*_{tap}$	(166 → 176)	0.025	3.99
306	^{1}MLCT	$4d_{Ru} \rightarrow \pi^*_{dppz}$	(170 → 181)	0.08	4.06
305	**^{1}MLCT**	$4d_{Ru} \rightarrow \pi^*_{dppz}$	(169 → 180)	**0.54**	**4.07**
304	^{1}IL	$\pi_{tap} \rightarrow \pi^*_{tap}$	(165 → 178)	0.01	4.07

[a] The molecular orbitals numbering refers to Fig. 2a.

and 300 nm. Whereas $[Ru(phen)_2dppz]^{2+}$ spectrum is characterized by a series of low-lying MLCT states ($4d_{Ru} \rightarrow \pi^*_{phen}$, $4d_{Ru} \rightarrow \pi^*_{dppz}$) close in energy between 435 nm and 411 nm, the $[Ru(tap)_2dppz]^{2+}$ absorption spectrum is more diversified: the lowest state corresponds to a ^{1}IL localized on the dppz ligand and is calculated at 429 nm, followed by a ^{1}MLCT state ($4d_{Ru} \rightarrow \pi^*_{tap}$) and a series of ^{1}LLCT states corresponding to charge transfer from dppz to tap, the most intense one at 401 nm. The next intense ^{1}IL transition is calculated at 382 nm with oscillator strength of 0.18. In contrast, in the phen complex the first ^{1}IL ($\pi_{ddpz} \rightarrow \pi^*_{dppz}$) transition is calculated at 411 nm and is followed by a second series of ^{1}MLCT states until 340 nm.

Looking at the oscillator strengths, the theoretical absorption spectrum of $[Ru(tap)_2dppz]^{2+}$ is characterized by four intense bands calculated at 401 nm (^{1}LLCT, $f = 0.1$), 382 nm (^{1}IL, $f = 0.18$), 324 nm (^{1}MLCT/^{1}IL, $f = 0.19$) and 305 nm (^{1}MLCT, $f = 0.54$). It is worth noting that the MLCT absorptions band corresponding to charge transfer to the dppz ligand are stronger than those corresponding to charge transfer to the tap ligand.

Table 5
TD-DFT transition energies (in nm and eV) of the low-lying absorbing states ($f > 0.01$) of $[Ru(phen)_2dppz]^{2+}$ and associated oscillator strengths f (in vacuum)

nm	Transition	One-electron excitation[a]		f	eV
435	^{1}MLCT	$4d_{Ru} \rightarrow \pi^*_{phen}$	(172 → 175)	0.01	2.85
423	^{1}MLCT	$4d_{Ru} \rightarrow \pi^*_{phen}$	(171 → 175)	0.04	2.93
419	^{1}MLCT	$4d_{Ru} \rightarrow \pi^*_{phen}$	(173 → 178)	0.02	2.96
416	^{1}MLCT	$4d_{Ru} \rightarrow \pi^*_{dppz}$	(171 → 177)	0.03	2.98
411	**^{1}MLCT**	$\mathbf{4d_{Ru} \rightarrow \pi^*_{dppz}}$	(172 → 177)	**0.20**	**3.02**
411	^{1}IL	$\pi_{dppz} \rightarrow \pi^*_{dppz}$	(174 → 177)	0.01	3.02
402	^{1}MLCT	$4d_{Ru} \rightarrow \pi^*_{phen}$	(173 → 179)	0.04	3.09
392	^{1}MLCT	$4d_{Ru} \rightarrow \pi^*_{phen}$	(172 → 178)	0.07	3.17
391	^{1}MLCT	$4d_{Ru} \rightarrow \pi^*_{phen}$	(171 → 178)	0.02	3.17
380	^{1}MLCT	$4d_{Ru} \rightarrow \pi^*_{phen}$	(171 → 179)	0.02	3.26
378	^{1}MLCT	$4d_{Ru} \rightarrow \pi^*_{phen}/4d_{Ru} \rightarrow \pi^*_{dppz}$	(171 → 176)/(171 → 177)	0.05	3.28
364	^{1}MLCT	$4d_{Ru} \rightarrow \pi^*_{dppz}$	(173 → 181)	0.02	3.40
342	^{1}MLCT	$4d_{Ru} \rightarrow \pi^*_{dppz}$	(172 → 181)	0.02	3.62
340	^{1}MLCT/^{1}LLCT	$4d_{Ru} \rightarrow \pi^*_{dppz}/\pi_{dppz} \rightarrow \pi^*_{phen}$	(171 → 181)/(170 → 175)	0.04	3.65
335	^{1}MC	$4d_{Ru} \rightarrow 4d_{Ru}$	(173 → 189)	0.01	3.69
332	^{1}IL	$\pi_{dppz} \rightarrow \pi^*_{dppz}$	(170 → 177)	0.02	3.72
316	^{1}LLCT	$\pi_{dppz} \rightarrow \pi^*_{phen}$	(170 → 179)	0.02	3.93
311	^{1}IL	$\pi_{phen} \rightarrow \pi^*_{phen}$	(168 → 175)	0.02	3.98
304	^{1}IL	$\pi_{dppz} \rightarrow \pi^*_{dppz}$	(170 → 181)	0.01	4.08
304	**^{1}IL**	$\mathbf{\pi_{dppz} \rightarrow \pi^*_{dppz}}$	(170 → 180)	**0.90**	**4.08**

[a] The molecular orbitals numbering refers to Fig. 2b.

As far as the intensities are concerned, only two strong bands are highlighted by the calculations in the absorption spectrum of $[Ru(phen)_2dppz]^{2+}$, namely a ^{1}MLCT calculated at 411 nm with $f=0.2$, and a ^{1}IL calculated at 304 nm with $f=0.9$. Again, the charge transfer states to the external ligand (phen in this case) are very weak.

A qualitative rationalization of the difference in the theoretical spectra of the two complexes can be explained as follows. When going from the phen to the tap complex the interaction between the $4d_{Ru}$ orbitals and the π^*_{dppz} is reduced due to the presence of an external ligand with a stronger π^* acceptor character. The main consequence is a stabilization of both $4d_{Ru}$ and π^*_{dppz} orbitals with a blue shift of the MLCT ($4d_{Ru} \rightarrow \pi^*_{dppz}$) states and a red shift of the IL ($\pi_{dppz} \rightarrow \pi^*_{dppz}$) states.

The theoretical absorption spectra of $[Ru(tap)_2dppz]^{2+}$ and $[Ru(phen)_2dppz]^{2+}$ in vacuum and solvent corrected (H_2O, CH_3CN) are compared to the experimental absorption data [13] in Table 6. The shoulder between 458 and 412 nm in the observed absorption spectrum of $[Ru(tap)_2dppz]^{2+}$ [13] can be assigned to the series of the low-lying ^{1}LLCT and ^{1}IL states (Table 4), from which the strongest peak is the ^{1}LLCT state calculated at 401 nm (Table 4). The strong absorption at 366–362 nm corresponds to a ^{1}IL calculated at 382 nm in vacuum. The intense band detected at 278 nm can be attributed to the ^{1}MLCT state calculated at 305 nm.

The lowest part of the absorption spectrum of $[Ru(phen)_2dppz]^{2+}$ is attributed to the ^{1}MLCT states calculated at 435 nm and 411 nm, in agreement to Ref [24]. The intense band observed in the far-UV energy domain beyond 300 nm can be assigned to the ^{1}IL transition calculated at 304 nm. As seen in Table 6, the absorption observed between these two well-defined bands, between 372 nm and 316 nm, corresponds to a series of ^{1}MLCT, ^{1}MLCT/^{1}LLCT, and ^{1}IL transitions, calculated between 402 nm and 311 nm in vacuum.

As illustrated by these results and in agreement with the experimental data reported in Table 3, the solvent corrections have little effect on transition energies at this level of calculation (electronic ground state optimized geometry in vacuum and PCM). The only large difference between the vacuum and solvent corrected spectra is the disappearance of the ^{1}MLCT/^{1}IL state calculated at 324 nm in vacuum for $[Ru(tap)_2dppz]^{2+}$. When solvent corrections are added this band vanishes and the lowest ^{1}IL state calculated at 382 nm with $f=0.18$ gains in intensity with an oscillator strength increasing to 0.3 (H_2O or CH_3CN). For both complexes the agreement between the experimental data and the solvent corrected transition energies is rather good and allows a satisfactory assignment of the electronic absorption spectra of $[Ru(tap)_2dppz]^{2+}$ and $[Ru(phen)_2dppz]]^{2+}$, representatives of a series of Ru(II) polypyridyl complexes used as intercalators in DNA for their potential light switch effect.

3.4. Photophysics and low-lying triplet states

The important difference in the electronic spectroscopy between $[Ru(tap)_2dppz]^{2+}$ and $[Ru(phen)_2dppz]^{2+}$ will have dramatic consequences on the photophysics of both compounds upon visible irradiation between 450 nm and 350 nm. Both systems are characterized by a high density of triplet states between 414 nm and 500 nm (Tables 7 and 8) to which the molecules may evolve via intersystem crossing (ISC) after absorption.

After irradiation of $[Ru(phen)_2dppz]^{2+}$ the low-lying ^{1}MLCT states calculated between 435 nm and 350 nm will be populated. As soon as the molecule has reached the emissive triplet MLCT states via ISC they are potentially active for light switch-on effect by virtue of luminescence (Scheme 1).

Irradiation of $[Ru(tap)_2dppz]^{2+}$ under the same conditions will excite the molecule to the low-lying ^{1}LLCT and ^{1}IL states. In particular the transition to the ^{1}IL state calculated at 382 nm and corresponding to a single excitation from a π_{dppz} orbital (numbered 173 in Fig. 2a) to the π^*_{dppz} orbital (numbered 179 in Fig. 2a) will create a very unstable intermediate $[Ru(II)(tap)_2(d^-ppz^+)]$ with an electronic deficiency on the external side of the dppz ligand, which can be potentially intercalated. Upon intercalation in DNA, this electronic deficiency will enhance the probability of reversible electron

Table 6
TD-DFT transition energies (in nm) in vacuum and solvent corrected (H_2O, CH_3CN) of the low-lying absorbing states ($f>0.1$) of $[Ru(tap)_2dppz]^{2+}$ and $[Ru(phen)_2dppz]^{2+}$ compared to the experimental absorption data [Ref. [13]] in water and acetonitrile

Experimental data H_2O/CH_3CN [26]	Transition	One-electron excitation	Vacuum	Solvent corrected H_2O	Solvent corrected CH_3CN
$[Ru(tap)_2dppz]^{2+}$					
412	^{1}LLCT	$\pi_{dppz} \rightarrow \pi^*_{tap}$	401 (*0.1*)	404 (*0.1*)	402 (*0.09*)
366/362	^{1}IL	$\pi_{dppz} \rightarrow \pi^*_{dppz}$	382 (*0.18*)	390 (*0.3*)	388 (*0.3*)
–	^{1}MLCT/^{1}IL	$4d_{Ru} \rightarrow \pi^*_{dppz}/\pi_{dppz} \rightarrow \pi^*_{dppz}$	324 (*0.19*)	–	–
278	^{1}MLCT	$4d_{Ru} \rightarrow \pi^*_{dppz}$	305 (*0.54*)	*294(0.6)*	*296 (1.1)*
$[Ru(phen)_2dppz]^{2+}$					
440	^{1}MLCT	$4d_{Ru} \rightarrow \pi^*_{phen}$	435 (*0.01*)	455 (*0.05*)	449 (*0.1*)
	^{1}MLCT	$4d_{Ru} \rightarrow \pi^*_{dppz}$	411 (*0.2*)	409 (*0.1*)	407 (*0.1*)
372–318/368 – 316	^{1}MLCT	$4d_{Ru} \rightarrow \pi^*_{phen}$	402 (*0.04*)	386 (*0.1*)	385 (*0.1*)
	^{1}MLCT/^{1}LLCT	$4d_{Ru} \rightarrow \pi^*_{dppz}/\pi_{dppz} \rightarrow \pi^*_{phen}$	340 (*0.04*)	337 (*0.1*)	338 (*0.1*)
	^{1}IL	$\pi_{phen} \rightarrow \pi^*_{phen}$	311 (*0.02*)	317 (<0.01)	316 (<0.01)
<300 nm	^{1}IL	$\pi_{dppz} \rightarrow \pi^*_{dppz}$	304 (*0.9*)	290 (*1.1*)	290 (*0.85*)

(Associated oscillator strengths *f* are given in parenthesis).

Table 7
TD-DFT transition energies (in nm and eV) of the low-lying triplet states of $[Ru(phen)_2dppz]^{2+}$

nm	Transition	One-electron excitation	eV
507	^{3}MLCT	$4d_{Ru} \rightarrow \pi^*_{phen}$	2.44
503	^{3}MLCT	$4d_{Ru} \rightarrow \pi^*_{phen}$	2.46
491	^{3}MLCT	$4d_{Ru} \rightarrow \pi^*_{phen}$	2.52
478	^{3}MLCT	$4d_{Ru} \rightarrow \pi^*_{phen}$	2.59
473	^{3}MLCT	$4d_{Ru} \rightarrow \pi^*_{dppz}$	2.61
463	^{3}MLCT	$4d_{Ru} \rightarrow \pi^*_{dppz}$	2.67
455	^{3}MLCT	$4d_{Ru} \rightarrow \pi^*_{phen}$	2.72
453	^{3}IL	$\pi_{dppz} \rightarrow \pi^*_{dppz}$	2.73
450	^{3}MLCT	$4d_{Ru} \rightarrow \pi^*_{phen}$	2.75
435	^{3}MLCT	$4d_{Ru} \rightarrow \pi^*_{phen}$	2.85
435	^{3}MLCT	$4d_{Ru} \rightarrow \pi^*_{phen}$	2.85
431	^{3}MLCT	$4d_{Ru} \rightarrow \pi^*_{dppz}$	2.87
426	^{3}IL/^{3}MLCT	$\pi_{dppz} \rightarrow \pi^*_{dppz}/4d_{Ru} \rightarrow \pi^*_{dppz}$	2.90
425	^{3}MLCT	$4d_{Ru} \rightarrow \pi^*_{phen}$	2.92
416	^{3}IL/^{3}LLCT	$\pi_{dppz} \rightarrow \pi^*_{dppz}/\pi_{dppz} \rightarrow \pi^*_{phen}$	2.97
414	^{3}MLCT	$4d_{Ru} \rightarrow \pi^*_{phen}$	2.99
399	^{3}MLCT	$4d_{Ru} \rightarrow \pi^*_{phen}$	3.11

Table 8
TD-DFT transition energies (in nm and eV) of the low-lying triplet states of $[Ru(tap)_2dppz]^{2+}$

nm	Transition	One-electron excitation	eV
582	^{3}IL	$\pi_{dppz} \rightarrow \pi^*_{dppz}$	2.13
520	^{3}MLCT	$4d_{Ru} \rightarrow \pi^*_{tap}$	2.37
517	^{3}MLCT	$4d_{Ru} \rightarrow \pi^*_{tap}$	2.40
502	^{3}MLCT	$4d_{Ru} \rightarrow \pi^*_{tap}$	2.47
489	^{3}LLCT	$\pi_{dppz} \rightarrow \pi^*_{tap}$	2.53
476	^{3}LLCT	$\pi_{dppz} \rightarrow \pi^*_{tap}$	2.60
470	^{3}LLCT	$\pi_{dppz} \rightarrow \pi^*_{tap}$	2.64
466	^{3}MLCT	$4d_{Ru} \rightarrow \pi^*_{tap}$	2.66
456	^{3}IL	$\pi_{dppz} \rightarrow \pi^*_{dppz}$	2.71
441	^{3}LLCT	$4d_{Ru} \rightarrow \pi^*_{tap}$	2.80
439	^{3}LLCT	$4d_{Ru} \rightarrow \pi^*_{tap}$	2.82
438	^{3}IL	$\pi_{dppz} \rightarrow \pi^*_{dppz}$	2.83
434	^{3}IL	$\pi_{dppz} \rightarrow \pi^*_{dppz}$	2.85
432	^{3}MLCT	$4d_{Ru} \rightarrow \pi^*_{tap}$	2.86
430	^{3}MLCT	$4d_{Ru} \rightarrow \pi^*_{dppz}$	2.88
427	^{3}IL	$\pi_{dppz} \rightarrow \pi^*_{dppz}$	2.90
423	^{3}MLCT	$4d_{Ru} \rightarrow \pi^*_{tap}$	2.93

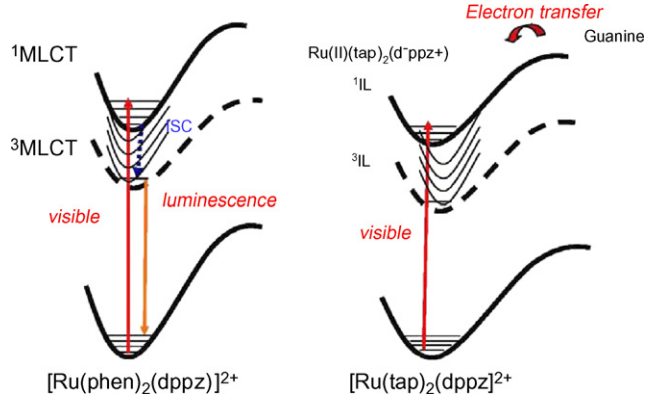

Scheme 1. Qualitative mechanism of deactivation of $[Ru(phen)_2(dppz)]^{2+}$ (left side) and $[Ru(tap)_2(dppz)]^{2+}$ (right side) after irradiation in the visible.

transfer from the guanine to the complex leading to the formation of the $G^{\bullet+}$ radical cation observed in various $[Ru(tap)L]^{2+}$ complexes (reaction 1). This competitive process will quench the light switch-on mechanism which can be efficiently activated only with the presence of an intense ^{1}MLCT band in the visible energy domain of the absorption spectrum. Note that the electron transfer process could also occur from the ^{3}IL state after $^1\text{IL} \rightarrow {}^3\text{IL}$ ISC, in a longer time scale.

The two extreme situations depicted in Scheme 1 represent two ideal scenarios. At the stage of this theoretical study, that is performed on the free molecules, direct connection with the great number of experimental data cannot be asserted. Indeed, the relative positions of the two low-lying singlet absorbing states playing a key role at the early stage after irradiation, namely the ^{1}IL and ^{1}MLCT states, will be controlled by the surrounding ligands and environmental effects (solvent, polynucleotide etc., ...). Consequently, under experimental conditions intermediate situations where both states can be populated can be expected. The branching ratio between the two competing processes, namely electron transfer from the guanine to the unstable $[Ru(II)(L)_2(d^-ppz^+)]$ intermediate versus intersystem crossing from the ^{1}MLCT state, will control the population of the low-lying ^{3}MLCT emissive states and consequently the quantum yield of luminescence.

4. Conclusion

The structures and electronic absorption spectra of $[Ru(phen)_2dppz]^{2+}$ and $[Ru(tap)_2dppz]^{2+}$, representative of a class of Ru(II) polypyridyl complexes used as intercalators in DNA for their molecular light switch properties have been calculated by means of density functional theory without and with solvent corrections for water and acetonitrile within the limit of the polarized continuum model. The solvent correction has a minor effect on the structures as well as on the absorption spectroscopy. The absorption spectrum of $[Ru(phen)_2dppz]^{2+}$ is characterized by the presence of a high density of low-lying MLCT ($4d_{Ru} \rightarrow \pi^*_{dppz}$) states between 435 nm and 340 nm with one strong absorption calculated at 409 nm in water and assigned to the band centred at 440 nm. The next absorbing state corresponds to a ^{1}IL ($\pi_{dppz} \rightarrow \pi^*_{dppz}$) calculated at 290 nm (water correction) assigned to the strong band observed beyond 300 nm. The absorption spectrum of the tap substituted complex $[Ru(tap)_2dppz]^{2+}$ is very different, showing the first strongly MLCT absorbing state calculated at 294 nm (water corrected) and assigned to the strong band observed at 278 nm. The ^{1}IL state is shifted to the visible energy domain at 390 nm (water corrected) and assigned to the band centred at 366 nm. It is shown that this difference in the absorption spectroscopy will have dramatic consequences on the photophysics of the two molecules potentially intercalated in DNA. After irradiation with visible light excited $[Ru(phen)_2dppz]^{2+*}$ will be formed in the ^{1}MLCT state. From there the system may evolve through intersystem crossing to the low-lying emissive ^{3}MLCT states leading to a light switch-on effect. In contrast, irradiation of $[Ru(tap)_2dppz]^{2+}$ in the same experimental conditions will populate the ^{1}IL state creating some electronic deficiency on the

external side of the dppz intercalated ligand by charge transfer from the π_{dppz} orbital localized on this side to a π^*_{dppz} orbital localized towards the metal centre. A very unstable species [Ru(II)(tap)$_2$(d$^-$ppz$^+$)], available for a competitive electron transfer from the guanine to the complex, will prevent emissive processes via the low-lying triplet states.

The rationalization of the photophysics of these two molecules constitutes an encouraging step towards the understanding of the molecular light switch effect in this class of compounds. The study of the specific influence of the polynucleotides on the spectroscopic and photophysical properties, in progress, is a computational challenge but is necessary to interpret the puzzle of unresolved experimental questions.

Acknowledgements

Dr. Leticia González wishes to thank the 'Berliner Förderprogram' for financial support. Dr. Michiko Atsumi is thankful to the joined JSPS program between Ochanomizu University and Université Louis Pasteur, to Dr. Yuasa Toshiko Memorial funds and to the French government. The European COST P9 Radiation Damage in Biomolecules is acknowledged. The calculations have been carried out at the LCQ (Strasbourg) and at the Institute for Molecular Science (Okazaki).

References

[1] E. Friedman, J.C. Chambron, J.P. Sauvage, N.J. Turro, J.K. Barton, J. Am. Chem. Soc. 112 (1990) 4960.
[2] R.M. Hartshorn, J.K. Barton, J. Am. Chem. Soc. 114 (1992) 5919, and references therein.
[3] Y. Jenkins, A.E. Friedman, N.J. Turro, J.K. Barton, Biochemistry 31 (1992) 10809.
[4] E.J.C. Olson, D. Hu, A. Hörmann, A.M. Jonkman, M.R. Arkin, E.D.A. Stemp, J.K. Barton, P.F. Barbara, J. Am. Chem. Soc. 119 (1997) 11458.
[5] C.G. Coates, J. Olofsson, M. Coletti, J.J. MacGarvey, B. Önfelt, P. Lincoln, B. Norden, E. Tuite, P. Matousek, A.W. Parker, J. Phys. Chem. B 105 (2001) 12653.
[6] J. Olofsoon, B. Önfelt, P. Lincoln, J. Phys. Chem. A 108 (2004) 4391.
[7] J.G. Vos, J.M. Kelly, Dalton Trans. (2006) 4869.
[8] P. Lincoln, A. Broo, B. Nordén, J. Am. Chem. Soc. 118 (1996) 2644.
[9] P. Lincoln, B. Nordén, J. Phys. Chem. B 102 (1998) 9583.
[10] B.H. Yun, J.O. Kim, B.W. Lee, P. Lincoln, B. Nordén, J. Phys. Chem. B 107 (2003) 9858.
[11] L. Jacquet, R.J.H. Davies, A. Kirsch-De Mesmaeker, J.M. Kelly, J. Am. Chem. Soc. 119 (1997) 11763.
[12] J.M. Kelly, C.M. Creely, M.M. Feeney, S. Hudson, W.J. Blau, Central Laser Facility Annual Report 2001/2002, pp. 111–114.
[13] C. Moucheron, A. Kirsch-De Mesmaeker, J. Phys. Org. Chem. 11 (1998) 577.
[14] C. Hiort, P. Lincoln, B. Nordén, J. Am. Chem. Soc. 115 (1993) 3448.
[15] Y. Lao, A. Chouai, N.N. Degtyareva, D.A. Lutterman, K.R. Dunbar, C. Turro, J. Am. Chem. Soc. 127 (2005) 10796.
[16] J.-C. Chambron, J.-P. Sauvage, Chem. Phys. Lett. 182 (1991) 603.
[17] V.W.W. Yam, K.K.-W. Lo, K.K. Cheung, R.Y. Kong, Chem. Comm. 11 (1995) 1191.
[18] R.B. Nair, B. Cullum, C.J. Murphy, Inorg. Chem. 36 (1997) 962.
[19] J. Olofsson, L.M. Wilhelmsson, P. Lincoln, J. Am. Chem. Soc. 126 (2004) 15458.
[20] S.J. Moon, J.M. Kim, J.Y. Choi, S.K. Kim, J.S. Lee, H.G. Jang, J. Inorg. Biochem. 99 (2005) 994.
[21] D. Han, H. Wang, N. Ren, J. Mol. Struct. (Theochem) 711 (2004) 185.
[22] A. Broo, P. Lincoln, Inorg. Chem. 36 (1997) 2544.
[23] G. Pourtois, D. Beljonne, C. Moucheron, S. Schumm, A. Kirsch-De Mesmaeker, R. Lazzaroni, J.L. Brédas, J. Am. Chem. Soc. 126 (2004) 683.
[24] S. Fantacci, F. De Angelis, A. Sgamellotti, N. Re, Chem. Phys. Lett. 396 (2004) 43.
[25] E.R. Batista, R.L. Martin, J. Phys. Chem. A 109 (2005) 3128.
[26] C. Lee, W. Yang, R.G. Parr, Phys. Rev. B37 (1988) 385.
[27] T.H. Dunning Jr., P.J. Hay, in: H.F. Schaefer III (Ed.), Modern Theoretical Chemistry, 3, Plenum, NY, 1976, p. 1.
[28] P.J. Hay, W.R. Wadt, J. Chem. Phys. 82 (1985) 270;
W.R. Wadt, P.J. Hay, J. Chem. Phys. 82 (1985) 284.
[29] P.C. Hariharan, J.A. Pople, Theor. Chim. Acta 28 (1973) 213;
M.M. Franci, W.J. Pietro, W.J. Hehre, J.S. Binkley, M.S. Gordon, D.J. DeFrees, J.A. Pople, J. Chem. Phys. 77 (1982) 3654.
[30] D. Andrae, U. Haussermann, M. Dolg, H. Preuss, Theor. Chim. Acta 77 (1990) 123.
[31] M.E. Casida, C. Jamorski, K.C. Casida, D.R. Salahub, J. Chem. Phys. 108 (1998) 4439.
[32] Y. Zhang, Z. Guo, X.-Z. You, J. Am. Chem. Soc. 123 (2001) 9378, and references therein.
[33] A. Dreuw, M. Head-Gordon, J. Am. Chem. Soc. 126 (2004) 4007.
[34] A. Dreuw, M. Head-Gordon, Chem. Rev. 105 (2005) 4009.
[35] O. Gritsenko, E.J. Barerends, J. Chem. Phys. 121 (2004) 655.
[36] C. Daniel, in: H. Yersin (Ed.), Topics in Current Chemistry, Springer-Verlag Heidelberg, vol. 241, Transition Metal and Rare Earth Compounds: Excited States, Transitions, Interactions III, 2005, pp. 119–165.
[37] C. Daniel, Photochemistry of transition metal complexes: theory, in: R. Crabtree (Ed.), Encyclopedia of Inorganic Chemistry, second ed., Wiley, UK, 2005.
[38] J. Bossert, C. Daniel, Chem. A Eur. J. 12 (2006) 4835.
[39] M. Turki, C. Daniel, S. Zalis, A. Vlcek, J. van Slageren, D.J. Stufkens, J. Am. Chem. Soc. 123 (2001) 11431.
[40] S. Zális, N. Ben Amor, C. Daniel, Inorg. Chem. 43 (2004) 7978.
[41] N. Ben Amor, S. Záliš, C. Daniel, Int. J. Quantum Chem. 106 (2006) 2458.
[42] J. Bossert, Ph.D. thesis, Université Louis Pasteur Strasbourg, 2005; J. Bossert, C. Daniel, Inorg. Chem. 2006, in preparation.
[43] M.T. Cancés, B. Mennucci, J. Tomasi, J. Chem. Phys. 107 (1997) 3032.
[44] M. Cossi, V. Barone, B. Bennucci, J. Tomasi, Chem. Phys. Lett. 286 (1998) 253.
[45] B. Bennucci, J. Tomasi, J. Chem. Phys. 106 (1997) 5151.
[46] Gaussian 03, Revision C.02, M.J. Frisch, G.W. Trucks, H.B. Schlegel, G.E. Scuseria, M.A. Robb, J.R. Cheeseman, J.A. Montgomery Jr., T. Vreven, K.N. Kudin, J.C. Burant, J.M. Millam, S.S. Iyengar, J. Tomasi, V. Barone, B. Mennucci, M. Cossi, G. Scalmani, N. Rega, G.A. Petersson, H. Nakatsuji, M. Hada, M. Ehara, K. Toyota, R. Fukuda, J. Hasegawa, M. Ishida, T. Nakajima, Y. Honda, O. Kitao, H. Nakai, M. Klene, X. Li, J.E. Knox, H.P. Hratchian, J.B. Cross, V. Bakken, C. Adamo, J. Jaramillo, R. Gomperts, R.E. Stratmann, O. Yazyev, A.J. Austin, R. Cammi, C. Pomelli, J.W. Ochterski, P.Y. Ayala, K. Morokuma, G.A. Voth, P. Salvador, J.J. Dannenberg, V.G. Zakrzewski, S. Dapprich, A.D. Daniels, M.C. Strain, O. Farkas, D.K. Malick, A.D. Rabuck, K. Raghavachari, J.B. Foresman, J.V. Ortiz, Q. Cui, A.G. Baboul, S. Clifford, J. Cioslowski, B.B. Stefanov, G. Liu, A. Liashenko, P. Piskorz, I. Komaromi, R.L. Martin, D.J. Fox, T. Keith, M.A. Al-Laham, C.Y. Peng, A. Nanayakkara, M. Challacombe, P.M.W. Gill, B. Johnson, W. Chen, M.W. Wong, C. Gonzalez, and J.A. Pople, Gaussian, Inc., Wallingford, CT, 2004. C. Lee, W. Yang, R.G. Parr, Phys. Rev. B37 (1988) 385.
[47] C. Piccinni-Leopardi, M. van Meerssche, J.P. Declercq, G. Germain, Bull. Soc. Chim. Belg. 96 (1987) 79.
[48] J.G. Liu, Q.L. Zhang, X.F. Shi, L.N. Ji, Inorg. Chem. 40 (2001) 5045.